Stoner Ferromagnetism in a Momentum-Confined Interacting 2D Electron Gas

Ohad Antebi, Ady Stern, and Erez Berg
Department of Condensed Matter Physics, Weizmann Institute of Science, Rehovot 76100, Israel

(Received 18 June 2023; revised 11 November 2023; accepted 19 January 2024; published 22 February 2024)

In this work we investigate the ground state of a momentum-confined interacting 2D electron gas, a momentum-space analog of an infinite quantum well. The study is performed by combining analytical results with a numerical exact diagonalization procedure. We find a ferromagnetic ground state near a particular electron density and for a range of effective electron (or hole) masses. We argue that this observation may be relevant to the generalized Stoner ferromagnetism recently observed in multilayer graphene systems. The collective magnon excitations exhibit a linear dispersion, which originates from a diverging spin stiffness.

DOI: 10.1103/PhysRevLett.132.086501

Introduction.—The ground state of a 2D electron gas is determined by a competition between kinetic and interaction energies. In the absence of external fields or ionic potentials, numerical calculations [1–5] suggest the ground state is either a paramagnetic Fermi liquid or a Wigner crystal [6], depending on the density, while a Stoner ferromagnetic [7] Fermi liquid state is a close competitor. By applying an out-of-plane magnetic field, the energy spectrum of the electron gas forms Landau levels. In the absence of Zeeman coupling the ground state is known to be ferromagnetic for densities near one electron per flux quantum [8,9].

Recent experiments in Bernal bilayer and rhombohedrally stacked multilayer graphene show spin and valley ferromagnetic phases for certain regimes of electron density and out-of-plane displacement field [10–15]. Furthermore, superconductivity has been experimentally demonstrated for the bilayer in Refs. [11,12,16] and the trilayer in Ref. [17], and theoretically discussed for various graphene multilayers in Refs. [18–29]. The band dispersion of the rhombohedrally stacked multilayer graphene systems is approximately flat up to some momentum scale, at which point the kinetic energy increases rapidly with momentum. This corresponds to a high density of states in a bounded region of momentum space, and is an example of a partially flat band. Here, we argue that such dispersion is favorable for Stoner ferromagnetism when the flat region is nearly fully occupied. We summarize these results in Fig. 1. Examples of various correlated phenomena that had been previously studied on models with partially flat bands can be found in Refs. [30–35].

Motivated by multilayer rhombohedrally stacked graphene, we present a toy model for an interacting 2D electron gas in which the kinetic energy of the electrons diverges beyond a limited region in momentum space. We will refer to this as a momentum-confined gas. We find the ground state of this gas to be spin polarized. We find a linearly dispersing magnon branch of excitations, in contrast with the commonly predicted quadratic dispersion [36]. We trace this apparent anomaly to a divergence of the spin stiffness associated with the infinite slope of the kinetic energy dispersion. We show that the spin polarization is robust to an addition of weak dispersion to the kinetic energy within the allowed momentum region.

Hamiltonian.—Our goal is to construct a simple model that captures non-trivial interaction effects of electrons confined in momentum space, with a minimal set of parameters. We consider a 2D electron gas with an artificially constructed kinetic dispersion, and turn on the conventional Coulomb repulsion. We imagine the kinetic dispersion to be such that the electrons are only allowed to occupy momenta in a disk of radius k_0 in momentum space, whose area is small compared to the Brillouin zone. Idealizing the dispersion, we set the kinetic energy to zero within the disk and to infinity outside it:

$$E_{\mathrm{K}}(\mathbf{k}) = \begin{cases} 0, & |\mathbf{k}| \le k_0, \\ \infty, & |\mathbf{k}| > k_0. \end{cases} \tag{1}$$

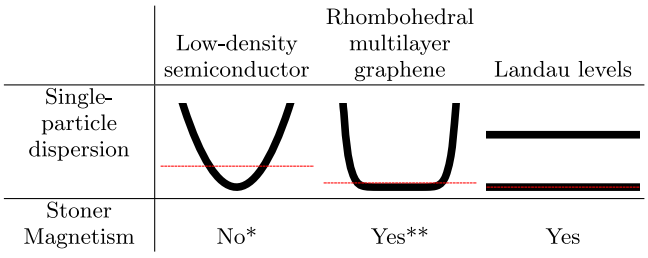

FIG. 1. Comparison of dispersion and Stoner ferromagnetism between different 2D systems. The dashed horizontal line represents the chemical potential. *Based on state of the art quantum Monte Carlo studies [5]. **Experimentally known for bilayer [11–14] and trilayer [10] graphene, both with a strong perpendicular displacement field, and analytically shown in this work for infinitely many layers.

This dispersion leads to the strict confinement of the electrons to a disk in momentum space, forming a momentum space analog of a 2D circular infinite quantum well in real space.

The confinement in Eq. (1) can be thought of as mimicking the low energy band dispersion of N_l layers of rhombohedral graphite subject to a displacement field D. For this system, there is a band gap proportional to D, the dispersion is very flat up to a momentum scale k_0, and rises as $E(k) \sim (k/k_0)^{N_l}$ for $k > k_0$. We emphasize that we are interested in an isolated band, and therefore consider $D \neq 0$ in this picture. In the limit of $N_l \to \infty$, the scale k_0 is set by the ratio of the interlayer tunneling $t_\perp$ and the monolayer Dirac velocity v_D (see Supplemental Material [37]). In this limit, the dispersion resembles the idealized momentum confined model of Eq. (1).

Next, we examine the effects of electron-electron interactions in such a momentum-confined setup. We consider our Hamiltonian to be the normal-ordered 2D screened Coulomb interaction strictly confined in momentum space:

$$\mathcal{H}_{\text{int}} = \frac{1}{2A}\sum_{\mathbf{q}} V_{\mathbf{q}} :\overline{\rho_{\mathbf{q}}}^{\dagger}\overline{\rho_{\mathbf{q}}}: , \tag{2}$$

$$\overline{\rho_{\mathbf{q}}} = \sum_{\sigma=\uparrow,\downarrow}\sum_{\mathbf{k}\in D_{\mathbf{q}}} c^{\dagger}_{\sigma,\mathbf{k}+\mathbf{q}} c_{\sigma,\mathbf{k}}, \tag{3}$$

where $c_{\sigma,\mathbf{k}}$ annihilates an electron with spin $\sigma \in \{\uparrow,\downarrow\}$ and momentum $\mathbf{k}$, A is the system area, $V_{\mathbf{q}} = 2\pi e^2 \tanh(|\mathbf{q}|d)/|\mathbf{q}|$ is the Fourier transform of the Coulomb potential, and d is the distance to the screening gate. The sum over momenta in the confined particle density operator, $\overline{\rho_{\mathbf{q}}}$, is limited to the domain $D_{\mathbf{q}} = \{\mathbf{k}|(|\mathbf{k}| \le k_0) \cap (|\mathbf{k}+\mathbf{q}| \le k_0)\}$ such that the fermion operators are within the disk of radius k_0 (see Fig. 2). While this Hamiltonian has only two (spin) flavors, some of the conclusions we draw below are applicable also in the presence of multiple valleys. We remark that any physical realization of the kinetic dispersion would be accompanied by form factors in Eq. (3) that originate from the Bloch wave functions. For simplicity, in this work we set the form factors to one.

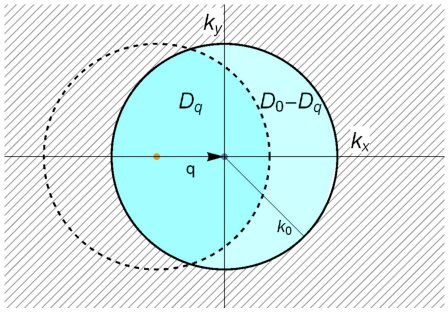

FIG. 2. The kinetic dispersion confines electrons to the disk D_0 of radius k_0 in momentum space. The region $D_{\mathbf{q}}$ is the intersection of two disks mutually shifted by $\mathbf{q}$. The strict momentum confinement forbids electrons with momenta in $D_0 - D_{\mathbf{q}}$ from scattering with a momentum transfer $\mathbf{q}$.

The Hamiltonian in Eq. (2) is the one we will explore for the rest of the paper. It has a continuous rotational symmetry around $\mathbf{k} = 0$, and a global $SU(2)$ symmetry for spin rotations. The most interesting property emerges in the limit of unscreened Coulomb interaction, $k_0 d \to \infty$. In this limit, the Hamiltonian has only one length scale, given by $l \sim k_0^{-1}$. Consequently, we find a single energy scale $E \sim e^2 k_0$, and an electron density scale $n_0 = k_0^2/(4\pi)$, which corresponds to completely filling the disk with a single spin flavor. Defining the filling factor by $\nu = n/n_0$, we will focus our discussion in this Letter on $\nu = 1$ and on $\nu = 1 \pm \varepsilon$ for $0 < \varepsilon \ll 1$.

The role of normal-ordering.—The notion of the single-particle kinetic dispersion in the presence of many-body interactions is not without subtleties. In our model, the flat nature of the dispersion is tied to our choice to consider the normal-ordered form of the interaction operator. Physically, the normal-ordering prevents an electron from interacting with itself. By undoing the normal ordering of the confined Coulomb interaction, we find that Eq. (2) can be separated into a positive semi-definite density-density operator and a single-particle operator:

$$\mathcal{H}_{\text{int}} = \underbrace{\frac{1}{2A}\sum_{\mathbf{q}} V_{\mathbf{q}}\overline{\rho_{\mathbf{q}}}^{\dagger}\overline{\rho_{\mathbf{q}}}}_{=\mathcal{H}_{\rho-\rho}} - \sum_{\sigma=\uparrow,\downarrow}\sum_{|\mathbf{k}|\le k_0} E_0(\mathbf{k}) c^{\dagger}_{\sigma,\mathbf{k}} c_{\sigma,\mathbf{k}}, \tag{4}$$

where we introduced the dispersion

$$E_0(\mathbf{k}) = \frac{1}{2A}\sum_{|\mathbf{k}'|\le k_0} V_{\mathbf{k}-\mathbf{k}'}. \tag{5}$$

This dispersion is, up to a sign, the exchange contribution to the self-energy of a particle at momentum $\mathbf{k}$ in the presence of a completely filled disk of radius k_0. In contrast with the standard unconfined interaction, we find that the momentum cutoff introduces a nontrivial dispersion term associated with the normal ordering. The dispersion in Eq. (5) plays an important role in several properties of our model and thus warrants an explicit discussion. In the limit of unscreened interaction, $k_0 d \to \infty$, this dispersion is given by

$$E_0(\mathbf{k}) = e^2 k_0 \frac{1}{\pi}\tilde{E}\left(\frac{\pi}{2}, \frac{|\mathbf{k}|}{k_0}\right), \tag{6}$$

where $\tilde{E}(\pi/2, x)$ is the complete elliptic integral of the second kind whose argument x is the elliptic modulus. The derivative of Eq. (6) diverges logarithmically at $|\mathbf{k}| = k_0$. This divergence is cut off for finite $k_0 d$. Expanding Eq. (5)

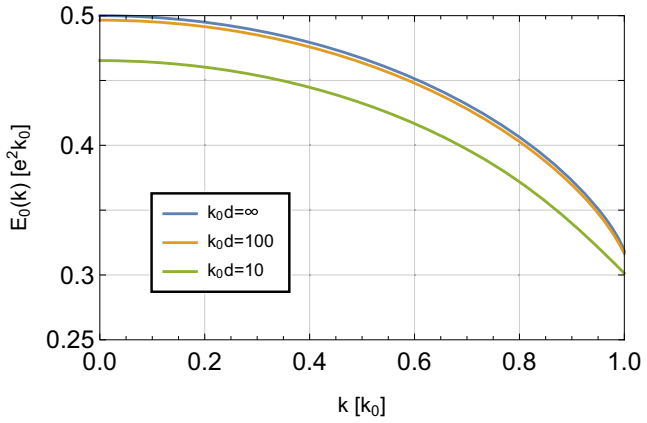

FIG. 3. The dispersion $E_0(|\mathbf{k}|)$ for different screening lengths of the Coulomb interaction. In the case of unscreened Coulomb interaction ($k_0 d \to \infty$) the dispersion is singular at $k = k_0$. This singularity is smoothed out for screened Coulomb interaction.

in $(k_0 d)^{-1}$, we find that the series does not uniformly converge on the disk, but nevertheless, the correction is small everywhere for $k_0 d \gg 1$. The effect of screening length on the dispersion is plotted in Fig. 3. The details are described in the Supplemental Material [37].

Exact ground state.—The ground state of Eq. (2) is not analytically solvable. We can, however, solve for the exact ground state upon introducing a particular dispersion to the otherwise flat disk, which would eliminate the contribution of Eq. (5). With this dispersion, we are left with the density-density Hamiltonian $\mathcal{H}_{\rho-\rho}$ as defined in Eq. (4). The Hamiltonian $\mathcal{H}_{\rho-\rho}$ is positive semi-definite, which provides a direct route to finding its exact ground state. For $\nu = 1$, consider completely filling the spin $\sigma = \downarrow$ flavor, i.e., a maximally spin-polarized state. We denote this state by $|\Psi_{\mathrm{SP}}\rangle$. By applying Eq. (3) one easily finds that

$$\forall\, \mathbf{q}\colon \overline{\rho_{\mathbf{q}}}|\Psi_{\mathrm{SP}}\rangle = 0 \Rightarrow \mathcal{H}_{\rho-\rho}|\Psi_{\mathrm{SP}}\rangle = 0, \tag{7}$$

which proves that $|\Psi_{\mathrm{SP}}\rangle$ is a ground state of $\mathcal{H}_{\rho-\rho}$. We emphasize that this ground state is degenerate with $SU(2)$ spin rotation symmetry. For a model with multiple valleys, the above statement holds for any integer filling ν and any completely spin- and valley-polarized state, provided that a large momentum separation between different valleys allows for a neglect of intervalley scattering in Coulomb processes.

The spin-polarized state $|\Psi_{\mathrm{SP}}\rangle$ is also an eigenstate of $\mathcal{H}_{\mathrm{int}}$. We *hypothesize* that $|\Psi_{\mathrm{SP}}\rangle$ is a ground state of $\mathcal{H}_{\mathrm{int}}$. We provide numerical evidence for this claim below. Assuming this hypothesis is correct, we proceed to calculate the excitations with respect to this state.

Single-particle excitations.—The single electron and hole excitations energies relative to the fully spin $\sigma = \downarrow$ polarized state, $E_e(\mathbf{k})$ and $E_h(\mathbf{k})$, respectively, are defined by

$$\begin{aligned}[\mathcal{H}_{\mathrm{int}}, c^\dagger_{\uparrow,\mathbf{k}}]|\Psi_{\mathrm{SP}}\rangle &= E_e(\mathbf{k}) c^\dagger_{\uparrow,\mathbf{k}}|\Psi_{\mathrm{SP}}\rangle,\\ [\mathcal{H}_{\mathrm{int}}, c_{\downarrow,\mathbf{k}}]|\Psi_{\mathrm{SP}}\rangle &= E_h(\mathbf{k}) c_{\downarrow,\mathbf{k}}|\Psi_{\mathrm{SP}}\rangle,\end{aligned} \tag{8}$$

and by direct calculation are found to be

$$\begin{aligned}E_e(\mathbf{k}) &= \frac{1}{A}\sum_{|\mathbf{k}'|\le k_0} V_{\mathbf{0}},\\ E_h(\mathbf{k}) &= \frac{1}{A}\sum_{|\mathbf{k}'|\le k_0} (V_{\mathbf{k}-\mathbf{k}'} - V_{\mathbf{0}}).\end{aligned} \tag{9}$$

The identity $E_0(\mathbf{k}) = (E_e(\mathbf{k}) + E_h(\mathbf{k}))/2$ holds also if one adds a spin-independent single-particle dispersion to the Hamiltonian $\mathcal{H}_{\mathrm{int}}$. The electron excitation energy is the charging energy of the system's geometric capacitance, and thus has a flat dispersion. The hole excitation energy has the same contribution (with an opposite sign), along with the exchange interaction of the missing electron. The dispersion of the hole excitation energy is therefore shown in Fig. 3 up to a factor of 2. We find that the hole dispersion is such that the lowest energy is obtained by removing a hole from the edge of the disk, thereby reducing the Fermi sea radius by an infinitesimal amount. This is identical to the Fermi liquid behavior.

Collective excitations.—The collective particle-hole excitations of momentum $\mathbf{Q}$ and spin $\hbar$ with respect to $|\Psi_{\mathrm{SP}}\rangle$ are eigenstates of $\mathcal{H}_{\mathrm{int}}$ spanned by wave functions of the form

$$|\Psi^{\mathbf{k},\mathbf{Q}}_{\mathrm{ph}}\rangle = c^\dagger_{\uparrow,\mathbf{k}+\mathbf{Q}} c_{\downarrow,\mathbf{k}}|\Psi_{\mathrm{SP}}\rangle. \tag{10}$$

We remark the state described by $|\Psi_{\mathrm{SP}}\rangle$ does not admit particle-hole excitations that are spinless, in contrast with the Stoner metallic state, and in some similarity to a ferromagnetic band insulator. The solution is given by diagonalizing the following matrix:

$$[H(\mathbf{Q})]_{\mathbf{k},\mathbf{k}'} = \langle \Psi^{\mathbf{k}',\mathbf{Q}}_{\mathrm{ph}}|\mathcal{H}_{\mathrm{int}}|\Psi^{\mathbf{k},\mathbf{Q}}_{\mathrm{ph}}\rangle, \qquad \mathbf{k},\mathbf{k}' \in D_{\mathbf{Q}}. \tag{11}$$

This restriction of both indices to the domain $D_{\mathbf{Q}} = \{\mathbf{k}|(|\mathbf{k}| \le k_0) \cap (|\mathbf{k}+\mathbf{Q}| \le k_0)\}$ is due to our infinite kinetic energy dispersion for states with momentum outside the disk. This sharp cutoff leads to a striking result—the lowest-lying particle-hole excitation is massless. For small $|\mathbf{Q}|/k_0$ we find

$$E_{\mathrm{ph}}(\mathbf{Q}) \approx \frac{4E_0(k_0)}{\pi k_0}|\mathbf{Q}|. \tag{12}$$

This is surprising, as for a magnon we normally expect to find a finite spin stiffness ρ_s such that $E_{\mathrm{ph}}(\mathbf{Q}) \approx \rho_s|\mathbf{Q}|^2$. The above result holds in the presence of any rotationally symmetric single-particle dispersion [37].

To resolve this apparent discrepancy, we replace our strictly confining kinetic dispersion with the following:

$$\mathcal{H}_{\mathrm{K}} = U_{\mathrm{K}} \sum_{\sigma=\uparrow,\downarrow} \sum_{\mathbf{k}} \left(\frac{|\mathbf{k}|}{k_0} \right)^{N_D} c^{\dagger}_{\sigma,\mathbf{k}} c_{\sigma,\mathbf{k}}, \tag{13}$$

where U_{K} is chosen such that $0 < U_{\mathrm{K}} \ll e^2 k_0$. Under this softened momentum confinement the momentum summations are unconstrained since particles are allowed to be excited beyond the disk. We emphasize that in the limit of $N_D \to \infty$ our strictly confining kinetic dispersion is restored. For $N_D \gg 1$ we find, using second order perturbation theory, that the spin stiffness is finite, and the magnon dispersion is quadratic:

$$E_{\mathrm{ph}}(\mathbf{Q}) \approx \frac{1}{2} \frac{U_{\mathrm{K}}}{k_0^2} N_D |\mathbf{Q}|^2. \tag{14}$$

However, in the limit $N_D \to \infty$, the spin stiffness $\rho_s \sim N_D$ diverges. This leads to a breakdown of perturbation theory as $|\mathbf{Q}|/k_0$ can no longer be used as a small parameter [37].

Phase diagram near $\nu = 1$.—We have seen above that when removing electrons (or adding holes) to the spin-polarized ground state $|\Psi_{\mathrm{SP}}\rangle$, it is energetically favorable to start with the outermost states, thereby reducing the radius of the occupied disk. Consider removing a small fraction of the electrons from the system, i.e., setting the system at filling fraction $\nu = 1 - \varepsilon$ for $0 < \varepsilon \ll 1$. We now argue that the system has a spin-polarized Fermi liquid ground state for small enough $\varepsilon > 0$. In the limit of $\varepsilon \to 0$, the spin polarization is undiminished, and the system can be thought of as having a single species of particles (in this case, holes), with a single particle dispersion $E_h(\mathbf{k}) = 2E_0(\mathbf{k})$ and subject to the 2D screened Coulomb interaction. Partially filling this system leads to a circular Fermi surface. The finite interaction strength (due to screening) and the constraint to 2D imply a Fermi liquid ground state. Presumably, continuing to decrease the filling will eventually destroy the spin polarization, and we expect a phase transition to a spin-depolarized state.

When the dispersion is exactly flat ($N_D \to \infty$) there is difficulty making a similar argument for filling $\nu = 1 + \varepsilon$, as the single-electron excitation spectrum is completely flat. However, as previously discussed, the average of single-electron and single-hole excitation spectra is constrained to be $E_0(\mathbf{k})$. Therefore, upon introduction of some weak dispersion to the disk, for example—by setting N_D to a finite value, we expect both electron and hole sides to display a Fermi liquid phase by the exact same reasoning. Generally, we note that the system has no particle-hole symmetry with respect to $\nu = 1$.

Numerical analysis.—In order to support our hypothesis of a spin-polarized ground state, we have performed an exact diagonalization study of Eq. (2) for finite systems with either periodic or twisted boundary conditions at filling factor $\nu = 1$ for $N \in \{6, 7, 12, 13, 18, 19\}$ particles. The diagonalization is done using the matrix-free implicitly restarted Lanczos method. We find the ground state at $\nu = 1$ to be the fully spin-polarized state for all system sizes considered. Further technical details are given in the Supplemental Material [37].

To further solidify our claim, we have examined the robustness of the spin-polarized ground state to additional dispersion. We repeat the exact diagonalization at $\nu = 1$ for the confined Coulomb Hamiltonian $\mathcal{H}_{\mathrm{int}}$ in Eq. (2) with an additional quadratic dispersion ($\hbar = 1$):

$$\mathcal{H}_{\mathrm{int+mass}} = \mathcal{H}_{\mathrm{int}} + \sum_{\sigma=\uparrow,\downarrow} \sum_{|\mathbf{k}| \le k_0} \frac{|\mathbf{k}|^2}{2m_{\mathrm{eff}}} c^{\dagger}_{\sigma,\mathbf{k}} c_{\sigma,\mathbf{k}}. \tag{15}$$

In Fig. 4 we plot the total spin S of the ground state of Eq. (15) at $\nu = 1$ vs m_{eff}^{-1}, as the latter is swept from negative to positive values in increments of $m_0^{-1} = V_{k_0} N/(2Ak_0^2)$. The flat kinetic dispersion in Eq. (1) corresponds to $m_{\mathrm{eff}}^{-1} = 0$. For the range of finite systems we considered, we find that the ground state is fully spin polarized, i.e., $S = N/2$, for $-3m_0^{-1} \lesssim m_{\mathrm{eff}}^{-1} \lesssim 2m_0^{-1}$, with the precise phase boundaries slightly varying with system size. Outside the spin-polarized region we find the spin polarization drops sharply to a lower value which depends on system size. One can show that, for all system sizes considered, this residual spin polarization has precisely the value expected by Hund's rule applied to a partial filling of the highest shell of degenerate kinetic energy states [37]. We associate this result with a spin-unpolarized phase, and expect that in the thermodynamic limit we will obtain $S/N \to 0$ in this regime of parameters. The asymmetry of the spin-polarized regime boundary with respect to the sign of m_{eff}^{-1} is due to the lower exchange energy of the

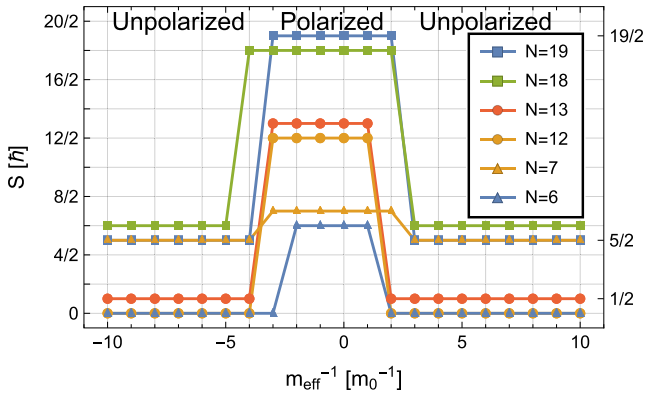

FIG. 4. The ground state spin polarization of the Hamiltonian in Eq. (15) at $\nu = 1$ as a function of inverse effective mass m_{eff}^{-1}, computed for various system sizes ranging from $N = 6$ to $N = 19$ particles. The horizontal axis increments are $m_0^{-1} = V_{k_0} N/(2Ak_0^2)$. The unpolarized phase has a subextensive polarization explained by Hund's rule.

unpolarized disk-shaped Fermi sea compared to that of an annular-shaped Fermi sea, the two different shapes that correspond to positive and negative m_{eff}^{-1}, respectively. In multilayer graphene systems with typical values of $k_0 = 0.2\ \mathrm{nm}^{-1}$ and dielectric coefficient $\epsilon_d = 6$, the mass scale is given by $m_0 \sim \epsilon_d k_0/e^2 \sim 0.06 m_e$ where m_e is the free electron mass.

Conclusions.—We considered a model of interacting electrons confined in momentum space, and showed that when nearly half of the available states are filled, its ground state is spin polarized. We then numerically demonstrated that this spin polarization is stable to small variations of the model, and is not a fine-tuned consequence of the kinetic dispersion. We find this ground state to have a nontrivial excitation spectrum, including a diverging spin stiffness which leads to massless particle-hole excitations at low momenta. We argued in favor of a ferromagnetic Fermi liquid phase at $\nu = 1 \pm \varepsilon$, thereby demonstrating Stoner ferromagnetism in this model. The prevalence of spin and valley Stoner ferromagnets in multilayer rhombohedral graphene in a displacement field, where for a range of densities electrons are confined to a flat region of momentum space, may be understood within the framework of our model.

O. A. would like to thank Johannes S. Hofmann, Daniel Kaplan, Tobias Holder, and Shahar Barkai for the useful discussions. We acknowledge support from the Israeli Science Foundation Quantum Science and Technology Grant No. 2074/19, and from the CRC 183 of the Deutsche Forschungsgemeinschaft (Project C02). This work has received funding from the European Research Council (ERC) under the European Union's Horizon 2020 research and innovation programme [Grant Agreements No. 788715 and 817799, Projects LEGOTOP (A. S.) and HQMAT (E. B.)].

[1] D. M. Ceperley and B. J. Alder, Ground state of the electron gas by a stochastic method, Phys. Rev. Lett. **45**, 566 (1980).
[2] B. Tanatar and D. M. Ceperley, Ground state of the two-dimensional electron gas, Phys. Rev. B **39**, 5005 (1989).
[3] F. Rapisarda and G. Senatore, Diffusion Monte Carlo study of electrons in two-dimensional layers, Aust. J. Phys. **49**, 161 (1996).
[4] C. Attaccalite, S. Moroni, P. Gori-Giorgi, and G. B. Bachelet, Correlation energy and spin polarization in the 2D electron gas, Phys. Rev. Lett. **88**, 256601 (2002).
[5] N. D. Drummond and R. J. Needs, Phase diagram of the low-density two-dimensional homogeneous electron gas, Phys. Rev. Lett. **102**, 126402 (2009).
[6] E. Wigner, On the interaction of electrons in metals, Phys. Rev. **46**, 1002 (1934).
[7] E. C. Stoner, Collective electron ferronmagnetism, Proc. R. Soc. London **165**, 372 (1938).
[8] K. Nomura and A. H. MacDonald, Quantum Hall ferromagnetism in graphene, Phys. Rev. Lett. **96**, 256602 (2006).
[9] S. M. Girvin, The quantum Hall effect: Novel excitations and broken symmetries, in *Aspects Topologiques de la Physique en Basse Dimension. Topological Aspects of Low Dimensional Systems* (Springer Berlin Heidelberg, Berlin, Heidelberg, 1999), pp. 53–175.
[10] H. Zhou, T. Xie, A. Ghazaryan, T. Holder, J. R. Ehrets, E. M. Spanton, T. Taniguchi, K. Watanabe, E. Berg, M. Serbyn, and A. F. Young, Half- and quarter-metals in rhombohedral trilayer graphene, Nature (London) **598**, 429 (2021).
[11] H. Zhou, L. Holleis, Y. Saito, L. Cohen, W. Huynh, C. L. Patterson, F. Yang, T. Taniguchi, K. Watanabe, and A. F. Young, Isospin magnetism and spin-polarized superconductivity in Bernal bilayer graphene, Science **375**, 774 (2022).
[12] Y. Zhang, R. Polski, A. Thomson, É. Lantagne-Hurtubise, C. Lewandowski, H. Zhou, K. Watanabe, T. Taniguchi, J. Alicea, and S. Nadj-Perge, Enhanced superconductivity in spin-orbit proximitized bilayer graphene, Nature (London) **613**, 268 (2023).
[13] S. C. de la Barrera, S. Aronson, Z. Zheng, K. Watanabe, T. Taniguchi, Q. Ma, P. Jarillo-Herrero, and R. Ashoori, Cascade of isospin phase transitions in Bernal-stacked bilayer graphene at zero magnetic field, Nat. Phys. **18**, 771 (2022).
[14] A. M. Seiler, F. R. Geisenhof, F. Winterer, K. Watanabe, T. Taniguchi, T. Xu, F. Zhang, and R. T. Weitz, Quantum cascade of correlated phases in trigonally warped bilayer graphene, Nature (London) **608**, 298 (2022).
[15] Y. Shi, S. Xu, Y. Yang, S. Slizovskiy, S. V. Morozov, S.-K. Son, S. Ozdemir, C. Mullan, J. Barrier, J. Yin *et al.*, Electronic phase separation in multilayer rhombohedral graphite, Nature (London) **584**, 210 (2020).
[16] L. Holleis, C. L. Patterson, Y. Zhang, H. M. Yoo, H. Zhou, T. Taniguchi, K. Watanabe, S. Nadj-Perge, and A. F. Young, Ising superconductivity and nematicity in Bernal bilayer graphene with strong spin orbit coupling, arXiv:2303.00742.
[17] H. Zhou, T. Xie, T. Taniguchi, K. Watanabe, and A. F. Young, Superconductivity in rhombohedral trilayer graphene, Nature (London) **598**, 434 (2021).
[18] O. A. Awoga, T. Löthman, and A. M. Black-Schaffer, Superconductivity and magnetism in the surface states of ABC-stacked multilayer graphene, Phys. Rev. B **108**, 144504 (2023).
[19] S. Chatterjee, T. Wang, E. Berg, and M. P. Zaletel, Intervalley coherent order and isospin fluctuation mediated superconductivity in rhombohedral trilayer graphene, Nat. Commun. **13**, 6013 (2022).
[20] Y.-Z. Chou, F. Wu, J. D. Sau, and S. Das Sarma, Acoustic-phonon-mediated superconductivity in rhombohedral trilayer graphene, Phys. Rev. Lett. **127**, 187001 (2021).
[21] Y.-Z. You and A. Vishwanath, Kohn-Luttinger superconductivity and intervalley coherence in rhombohedral trilayer graphene, Phys. Rev. B **105**, 134524 (2022).
[22] A. Ghazaryan, T. Holder, M. Serbyn, and E. Berg, Unconventional superconductivity in systems with annular Fermi surfaces: Application to rhombohedral trilayer graphene, Phys. Rev. Lett. **127**, 247001 (2021).

[23] A. L. Szabó and B. Roy, Metals, fractional metals, and superconductivity in rhombohedral trilayer graphene, Phys. Rev. B **105**, L081407 (2022).
[24] T. Cea, P. A. Pantaleón, V. o. T. Phong, and F. Guinea, Superconductivity from repulsive interactions in rhombohedral trilayer graphene: A Kohn-Luttinger-like mechanism, Phys. Rev. B **105**, 075432 (2022).
[25] D.-C. Lu, T. Wang, S. Chatterjee, and Y.-Z. You, Correlated metals and unconventional superconductivity in rhombohedral trilayer graphene: A renormalization group analysis, Phys. Rev. B **106**, 155115 (2022).
[26] A. Ghazaryan, T. Holder, E. Berg, and M. Serbyn, Multilayer graphenes as a platform for interaction-driven physics and topological superconductivity, Phys. Rev. B **107**, 104502 (2023).
[27] N. B. Kopnin, M. Ijäs, A. Harju, and T. T. Heikkilä, High-temperature surface superconductivity in rhombohedral graphite, Phys. Rev. B **87**, 140503(R) (2013).
[28] W. A. Muñoz, L. Covaci, and F. M. Peeters, Tight-binding description of intrinsic superconducting correlations in multilayer graphene, Phys. Rev. B **87**, 134509 (2013).
[29] R. Ojajärvi, T. Hyart, M. A. Silaev, and T. T. Heikkilä, Competition of electron-phonon mediated superconductivity and stoner magnetism on a flat band, Phys. Rev. B **98**, 054515 (2018).
[30] A. Mielke, Ferromagnetism in single-band Hubbard models with a partially flat band, Phys. Rev. Lett. **82**, 4312 (1999).
[31] E. Tang and L. Fu, Strain-induced partially flat band, helical snake states and interface superconductivity in topological crystalline insulators, Nat. Phys. **10**, 964 (2014).
[32] E. W. Huang, M.-S. Vaezi, Z. Nussinov, and A. Vaezi, Enhanced correlations and superconductivity in weakly interacting partially flat-band systems: A determinantal quantum Monte Carlo study, Phys. Rev. B **99**, 235128 (2019).
[33] S. Sayyad, E. W. Huang, M. Kitatani, M.-S. Vaezi, Z. Nussinov, A. Vaezi, and H. Aoki, Pairing and non-Fermi liquid behavior in partially flat-band systems: Beyond nesting physics, Phys. Rev. B **101**, 014501 (2020).
[34] H. Aoki, Theoretical possibilities for flat band superconductivity, J. Supercond. Novel Magn. **33**, 2341 (2020).
[35] S. Sayyad, M. Kitatani, A. Vaezi, and H. Aoki, Nematicity-enhanced superconductivity in systems with a non-Fermi liquid behavior, J. Phys. Condens. Matter **35**, 245605 (2023).
[36] H. Watanabe, Counting rules of Nambu-Goldstone modes, Annu. Rev. Condens. Matter Phys. **11**, 169 (2020).
[37] See Supplemental Material at http://link.aps.org/supplemental/10.1103/PhysRevLett.132.086501 for a detailed discussion, which includes Refs. [38–43].
[38] H. Min and A. H. MacDonald, Chiral decomposition in the electronic structure of graphene multilayers, Phys. Rev. B **77**, 155416 (2008).
[39] F. Zhang, B. Sahu, H. Min, and A. H. MacDonald, Band structure of ABC-stacked graphene trilayers, Phys. Rev. B **82**, 1 (2010).
[40] S. A. Gershgorin, Uber die Abgrenzung der Eigenwerte einer Matrix, lzv. Akad. Nauk. USSR. Otd. Fiz-Mat. Nauk **7**, 749 (1931).
[41] R. S. Varga, *Geršgorin and His Circles* (Springer Science & Business Media, New York, 2011).
[42] R. B. Lehoucq, D. C. Sorensen, and C. Yang, *ARPACK Users' Guide: Solution of Large-Scale Eigenvalue Problems with Implicitly Restarted Arnoldi Methods* (Society for Industrial and Applied Mathematics, Philadelphia, 1998).
[43] opencollab, ARPACK-NG: A new generation of implicitly restarted Arnoldi library, https://github.com/opencollab/arpack-ng.